JOURNAL OF Materials CHEMISTRY

Synthesis and photocatalytic properties of layered $HNbWO_6$/(Pt, $Cd_{0.8}Zn_{0.2}S$) nanocomposites

Jihuai Wu,*[a] Jianming Lin,[a] Shu Yin[b] and Tsugio Sato[b]

[a]*Institute for Materials Physical Chemistry, Huaqiao University, Quanzhou, Fujian, 362011, P. R. China. E-mail: jhwu@hqu.edu.cn*
[b]*Institute for Chemical Reaction Science, Tohoku University, Sendai 980-8577, Japan*

Received 30th April 2001, Accepted 11th July 2001
First published as an Advance Article on the web 14th September 2001

$HNbWO_6$/(Pt,$Cd_{0.8}Zn_{0.2}S$) nanocomposites have been fabricated by successive intercalation reactions of $HNbWO_6$ with $[Pt(NH_3)_4]Cl_2$ aqueous solution, with n-$C_3H_7NH_2$/n-heptane mixed solution, and the $Cd(MeCO_2)_2$–$Zn(MeCO_2)_2$ mixture in aqueous solution, followed by the reaction between Cd^{2+}–Zn^{2+} and H_2S in the interlayer of $HNbWO_6$. The gallery height of $HNbWO_6$/CdS*, $HNbWO_6$/$Cd_{0.8}Zn_{0.2}S$*, $HNbWO_6$/CdS, $HNbWO_6$/$Cd_{0.8}Zn_{0.2}S$, $HNbWO_6$/(Pt, CdS) and $HNbWO_6$/(Pt,$Cd_{0.8}Zn_{0.2}S$) is less than 0.5 nm in each case. $HNbWO_6$/(Pt,$Cd_{0.8}Zn_{0.2}S$) series nanocomposites show a broad reflectance over *ca.* 380–580 nm and are capable of efficient hydrogen evolution under the irradiation of visible light in the presence of Na_2S as a sacrificial donor. The photocatalytic activities of $HNbWO_6$/CdS and $HNbWO_6$/$Cd_{0.8}Zn_{0.2}S$ nanocomposites are superior to those of unsupported CdS and $Cd_{0.8}Zn_{0.2}S$ and are enhanced by the the co-incorporation of Pt.

1 Introduction

Photoelectrochemical processes at the semiconductor colloid–electrolyte interface, such as the splitting of water and the reduction of carbon dioxide, have received special attention because of their application in the conversion of solar energy into chemical energy. A semiconductor with high solar energy conversion efficiency should have a band gap energy of less than 3 eV, which both covers the main part of the solar spectrum and is distributed within the visible light region. In general, however, photoactivities of semiconductors with a small band gap energy are modest. It is to be expected that the photoactivity of a semiconductor increases with a decrease in its particle size, since in such a system the distance the photoinduced holes and electrons must diffuse before reaching the interface decreases, and the holes and electrons can be effectively captured by the electrolyte in the solution.[1] On the other hand, the coupling of two semiconductor particles with different energy levels is useful to achieve effective charge separation. For example, in a colloidal CdS–TiO_2 system, a photogenerated electron can transfer from a CdS to a TiO_2 particle while the holes remain in the CdS particle.[2] The enhancement of hydrogen gas production from H_2S solution[3] and acceleration of methylviologen reduction[4] have been observed for the CdS–TiO_2 system. Incorporation of two semiconductors with different energy levels in the interlayer region of a lamellar compound is a promising method for the fabrication of a nanocomposite consisting of host layers with ultrafine particles in the interlayers. Enea and Bard,[5] Yoneyama and coworkers,[6–8] and Sato and coworkers[9–12] have reported the incorporation of extremely small particles of Fe_2O_3, TiO_2, CdS and a CdS–ZnS mixture, of less than 1 nm in thickness, into the interlayers of layered compounds such as montmorillonite, layered double hydroxides, layered niobate and layered titanate. As expected, the photocatalytic activities of the incorporated semiconductors were much higher than those of unsupported semiconductors. In previous papers,[11,12] we have reported preparation and photoactivities of $HNbWO_6$/TiO_2 and $HTaWO_6$/TiO_2. In continuation of our studies, new layered nanocomposites, $HNbWO_6$/$Cd_{0.8}Zn_{0.2}S$, have been synthesized and their photocatalytic activities evaluated.

2 Experimental

2.1 Chemical

$HNbWO_6$ was prepared by the proton exchange reaction of $LiNbWO_6$ in 2 M HNO_3 solution at room temperature for 48 h with one intermediate replacement of the acid in 24 h. $LiNbWO_6$ was obtained by calcining a stoichiometric mixture of Li_2CO_3, WO_3 and Nb_2O_5 at 800 °C in air for 24 h with grinding after 12 h of the calicnation.[13] CdS was prepared by the reaction between 0.5 M $Cd(MeCO_2)_2$ solution and 0.5 M Na_2S solution at room temperature; $Cd_{0.8}Zn_{0.2}S$ was prepared by the reaction between the 0.4 M $Cd(MeCO_2)_2$–0.1 M $Zn(MeCO_2)_2$ mixed solution and 0.5 M Na_2S solution at room temperature.

2.2 Preparation of $HNbWO_6$/$Cd_{0.8}Zn_{0.2}S$ and $HNbWO_6$/CdS nanocomposites

$HNbWO_6$ was converted into $HNbWO_6$/n-$C_3H_7NH_2$ by stirring $HNbWO_6$ (1 g) in 50 ml of 20 vol% n-$C_3H_7NH_2$/n-heptane organic solution under reflux at 50 °C for 72 h. $Cd_{0.8}Zn_{0.2}S$ and CdS particles were incorporated into the interlayer of $HNbWO_6$ by bubbling H_2S gas into the suspension of the Cd^{2+}–Zn^{2+}- and Cd^{2+}-exchanged compounds with stirring at room temperature for 2 h. The Cd^{2+}–Zn^{2+}- and Cd^{2+}-exchanged compounds were obtained by ion exchange reactions of $HNbWO_6$/n-$C_3H_7NH_2$ (4 g) with 0.4 M $Cd(MeCO_2)_2$–0.1 M $Zn(MeCO_2)_2$ mixed solution (100 ml) and with 0.5 M $Cd(MeCO_2)_2$ solution (100 ml), each under reflux at 50 °C for 72 h, respectively. The samples obtained were designated as $HNbWO_6$/$Cd_{0.8}Zn_{0.2}S$ and $HNbWO_6$/CdS. Preparation of the nanocomposites without expanding the interlayer of $HNbWO_6$ by n-$C_3H_7NH_2$ was also carried out. The samples thus obtained were designated as $HNbWO_6$/$Cd_{0.8}Zn_{0.2}S$* and $HNbWO_6$/CdS*.

DOI: 10.1039/b103838a

2.3 Incorporation of Pt in the interlayer of $HNbWO_6$ together with $Cd_{0.8}Zn_{0.2}S$

$[Pt(NH_3)_4]^{2+}$ was incorporated in the interlayer of $HNbWO_6$ by stirring $HNbWO_6$ (4 g) in 0.6 mM $[Pt(NH_3)_4]Cl_2$ aqueous solution (1000 ml) at room temperature for 72 h. After being filtered and washed with water, the specimen was dispersed in water and irradiated with UV light from a 450 W high-pressure mercury lamp at room temperature for 5 h in order to deposit Pt particles in the interlayer of $HNbWO_6$. After that $Cd_{0.8}Zn_{0.2}S$ particles were incorporated in the interlayer of $HNbWO_6$/Pt by successive intercalating reactions with $HNbWO_6$/Pt and 20 vol% n-$C_3H_7NH_2$/n-heptane organic solution, and with 0.4 M $Cd(MeCO_2)_2$–0.1 M $Zn(MeCO_2)_2$ mixed solution, followed by bubbling H_2S gas through the suspension in a similar manner as that for preparing $HNbWO_6$/$Cd_{0.8}Zn_{0.2}S$; the sample obtained was designated as $HNbWO_6$/(Pt, $Cd_{0.8}Zn_{0.2}S$). By using a similar method, the $HNbWO_6$/(Pt, CdS) was also obtained.

2.4 Analysis

The crystalline phases of the products were identified by X-ray diffraction (Rigaku Denki Geiger-flex 2013) using graphite monochromated Cu-Kα radiation. The chemical compositions of the samples were determined by TG–DTA analysis (Rigaku Denki TAS 200 TG–DTA) and by inductively coupled plasma (ICP) atomic emission spectroscopy (Seiko SPS-1200A) by dissolving the samples in water after adding 0.1 g samples to a HCl–HNO_3 (3 : 1) solution (100 ml) and boiling for 2 h. The band gap energies of the products were determined from the onset of diffuse reflectance spectra of the samples measured using a Shimadzu Model UV-2000 UV–VIS spectrophotometer. Specific surface areas of the samples were determined by the nitrogen gas adsorption method (Quantachrome Autosorb-1).

2.5 Photocatalytic reactions

Photocatalytic reactions were carried out in a Pyrex reactor of 1250 ml capacity attached to an inner radiation type 450 W high-pressure mercury arc lamp. The temperature of the inner cell was controlled *via* thermostatted water flowing through a jacket between the mercury lamp and the reaction chamber. The inner cell was constructed from Pyrex glass, which served to filter out UV emissions of the mercury arc with wavelengths of <290 nm. In order to filter out wavelengths of <400 nm a flowing 1 M thermostatted $NaNO_2$ solution was used between the mercury lamp and the reaction chamber. The photocatalytic activities of the samples were determined by measuring the volume of hydrogen gas evolved, using a gas burette, when the sample suspension was irradiated.

3 Results and discussion

3.1 Intercalation of CdS and $Cd_{0.8}Zn_{0.2}S$ into the interlayer of $HNbWO_6$

The thermogravimetric curve (shown in Fig. 1) of the Cd^{2+}-exchanged compound obtained by the reaction of $HNbWO_6$/$C_3H_7NH_2$ with $Cd(MeCO_2)_2$ [Fig. 1(a)] shows a weight loss of around 2.10% up to 1000 °C. The result is in accord with thecalculated value (2.05 wt%) according to the following reaction:

$$Cd(NbWO_6)_2{\cdot}H_2O + 5O_2 \rightarrow Nb_2O_5 + 2WO_3 + CdO + H_2O$$

On the other hand, the interlayer distance of the Cd^{2+}-exchanged compound determined by subtracting the thickness of the $NbWO_6^-$ layer, 0.76 nm,[13,14] from its interlayer distance with XRD (shown in Fig. 2) is 0.39 nm, which suggests that no $MeCO_2$ and $C_3H_7NH_2$ groups are incorporated into the interlayer of $HNbWO_6$ except Cd^{2+} and H_2O. Chemical analysis confirmed this by finding no $MeCO_2$ and $C_3H_7NH_2$ groups incorporated into the interlayer of $HNbWO_6$. Therefore the Cd^{2+}-exchanged compound might be suggested as $Cd(NbWO_6)_2{\cdot}H_2O$.

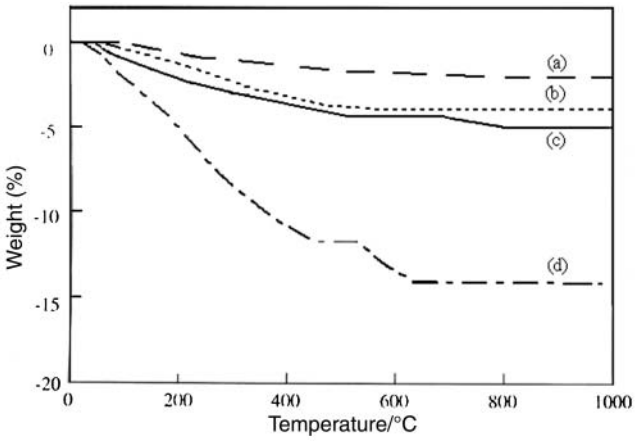

Fig. 1 TG curves of (a) $HNbWO_6$/CdO or $Cd(NbWO_6)_2{\cdot}H_2O$ [prepared by the reaction of $HNbWO_6$/$C_3H_7NH_2$ with $Cd(MeCO_2)_2$], (b) $HNbWO_6{\cdot}H_2O$, (c) $HNbWO_6$/CdS and (d) $HNbWO_6$/$C_3H_7NH_2$.

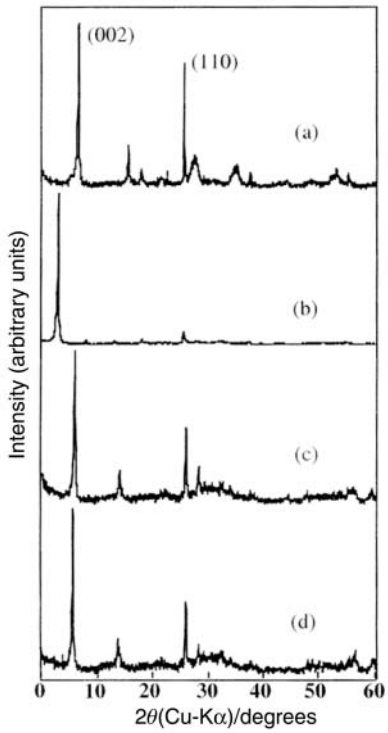

Fig. 2 Powder X-ray diffraction patterns of (a) $HNbWO_6$, (b) $HNbWO_6$/$C_3H_7NH_2$, (c) Cd^{2+}-exchanged compound prepared by the reaction of $HNbWO_6$/$C_3H_7NH_2$ with $Cd(MeCO_2)_2$, and (d) $HNbWO_6$/CdS.

From the content of Cd (12.1 wt%) measured by chemical composition analysis with ICP, the molar ratio of CdS : $HNbWO_6$ is *ca.* 1 : 2 in the $HNbWO_6$/CdS nanocomposite. On the other hand, the TG curve of the $HNbWO_6$/CdS nanocomposite [Fig. 1(c)] indicates a weight loss of *ca.* 5.0% up to 1000 °C which is close to the calculated value (5.6 wt%) according to the following reaction:

$$2HNbWO_6{\cdot}(CdS)_{1/2} + 10O_2 \rightarrow Nb_2O_5 + 2WO_3 + 2CdO + H_2O + SO_3$$

Therefore, it is believed that the molar ratio of CdS : $HNbWO_6$ is 1 : 2. Based on the above, the intercalation

process of CdS into $HNbWO_6$ might be written as follows:

$$HNbWO_6 + C_3H_7NH_2 \rightarrow C_3H_7NH_3^+ \cdot NbWO_6^-$$

$$2C_3H_7NH_3^+ \cdot NbWO_6^- + CdMeCO_2 \rightarrow Cd(NbWO_6)_2 \cdot H_2O + C_3H_7NH_3MeCO_2$$

$$Cd(NbWO_6)_2 \cdot H_2O + H_2S \rightarrow H_2O + HNbWO_6 \cdot (CdS)_{1/2} = HNbWO_6/CdS$$

Based on similar experiments, $HNbWO_6$/CdS, $HNbWO_6$/$Cd_{0.8}Zn_{0.2}S$, $HNbWO_6$/(Pt, CdS) and $HNbWO_6$/(Pt, $Cd_{0.8}Zn_{0.2}S$) nanocomposites were also found to have a molar ratio of incorporated semiconductor to host of 1 : 2. However, for the $HNbWO_6/CdS^*$ and $HNbWO_6/Cd_{0.8}Zn_{0.2}S^*$ nanocomposites, the molar ratio of incorporated semiconductor to host is less than 0.5 which indicates the ion exchange of Cd^{2+} and Zn^{2+}, and consequently the incorporation of CdS and ZnS is promoted by the pre-expansion of the interlayer with n-$C_3H_7NH_3^+$.

3.2 Properties of $HNbWO_6$/(Pt, $Cd_{0.8}Zn_{0.2}S$) series nanocomposites

The X-ray powder diffraction patterns of (a) $HNbWO_6$, (b) CdS, (c) $Cd_{0.8}Zn_{0.2}S$, (d) $HNbWO_6/CdS^*$, (e) $HNbWO_6$/$Cd_{0.8}Zn_{0.2}S^*$, (f) $HNbWO_6$/CdS, (g) $HNbWO_6$/$Cd_{0.8}Zn_{0.2}S$, (h) $HNbWO_6$/(Pt, CdS) and (i) $HNbWO_6$/(Pt, $Cd_{0.8}Zn_{0.2}S$) are shown in Fig. 3. The diffraction peak positions of samples (d)–(i), corresponding to the (110) crystal face of $HNbWO_6$, change, depending upon the species in the interlayer. These results suggest that the layered structure of $HNbWO_6$ is kept after intercalation of CdS, $Cd_{0.8}Zn_{0.2}S$ and Pt, although the interlayer distance changes. Samples (b) and (c) show a broad diffraction range corresponding to a zinc-blende structure, indicating the formation of a CdS and ZnS solid solution. Since the gallery heights for $HNbWO_6/CdS^*$, $HNbWO_6/Cd_{0.8}Zn_{0.2}S^*$, $HNbWO_6$/CdS, $HNbWO_6$/$Cd_{0.8}Zn_{0.2}S$, $HNbWO_6$/(Pt, CdS) and $HNbWO_6$/(Pt, $Cd_{0.8}Zn_{0.2}S$) were found to be in the approximate range 0.38–0.39 nm, it is suggested that the thickness of incorporated layer is <0.5 nm which indicates the formation of nanocomposites. It is notable that $HNbWO_6/CdS^*$, $HNbWO_6$/CdS and $HNbWO_6$/(Pt, CdS) have the same gallery height, 0.38 nm, although different preparation methods were applied and different particles incorporated into the interlayer of $HNbWO_6$. This similarity might be because the semiconductor incorporated into the above nanocomposites is CdS for all. On the other hand, owing to the same reasons, $HNbWO_6/Cd_{0.8}Zn_{0.2}S^*$, $HNbWO_6$/$Cd_{0.8}Zn_{0.2}S$ and $HNbWO_6$/(Pt, $Cd_{0.8}Zn_{0.2}S$) also have the same gallery height, 0.39 nm. The slightly higher interlayer distances for the $HNbWO_6$/$Cd_{0.8}Zn_{0.2}S$ nanocomposites seem to be attributable to the bigger ion radius of Cd compared with Zn.

Fig. 4 presents the diffuse reflectance spectra of (a) $HNbWO_6$, (b) CdS, (c) $Cd_{0.8}Zn_{0.2}S$, (d) $HNbWO_6/CdS^*$, (e) $HNbWO_6$/$Cd_{0.8}Zn_{0.2}S^*$, (f) $HNbWO_6$/CdS, (g) $HNbWO_6$/$Cd_{0.8}Zn_{0.2}S$, (h) $HNbWO_6$/(Pt, CdS) and (i) $HNbWO_6$/(Pt, $Cd_{0.8}Zn_{0.2}S$). Samples (d)–(i) all show broad reflectance spectra with two onsets corresponding to host $HNbWO_6$ and incorporated semiconductor CdS or $Cd_{0.8}Zn_{0.2}S$, respectively. The blue shift phenomenon of band gap energies between unsupported and incorporated semiconductors is observed in all six kinds of $HNbWO_6$/(Pt, CdS) series nanocomposites, such as the band gap energies of 1.99 and 2.25 eV corresponding to CdS in the unsupported compound and in $HNbWO_6$/CdS nanocomposites, respectively, which is consistent with the results of the quantum size effect of nanocomposites.[15] The blue shift phenomenon also occurs in host $HNbWO_6$. For instance, the band gap energy of the $HNbWO_6$ compound is 3.06 eV, but increases to 3.22 eV in the $HNbWO_6$/CdS nanocomposite. Slight and regular band gap energies different among $HNbWO_6/CdS^*$, $HNbWO_6$/CdS, $HNbWO_6$/(Pt, CdS) and among $HNbWO_6/Cd_{0.8}Zn_{0.2}S^*$, $HNbWO_6$/$Cd_{0.8}Zn_{0.2}S$

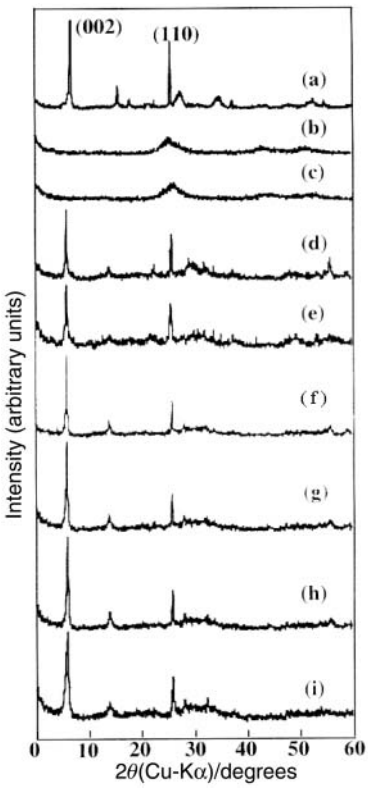

Fig. 3 Powder X-ray diffraction patterns of (a) $HNbWO_6$, (b) CdS, (c) $Cd_{0.8}Zn_{0.2}S$, (d) $HNbWO_6/CdS^*$, (e) $HNbWO_6$/$Cd_{0.8}Zn_{0.2}S^*$, (f) $HNbWO_6$/CdS, (g) $HNbWO_6$/$Cd_{0.8}Zn_{0.2}S$, (h) $HNbWO_6$/(Pt, CdS) and (i) $HNbWO_6$/(Pt, $Cd_{0.8}Zn_{0.2}S$).

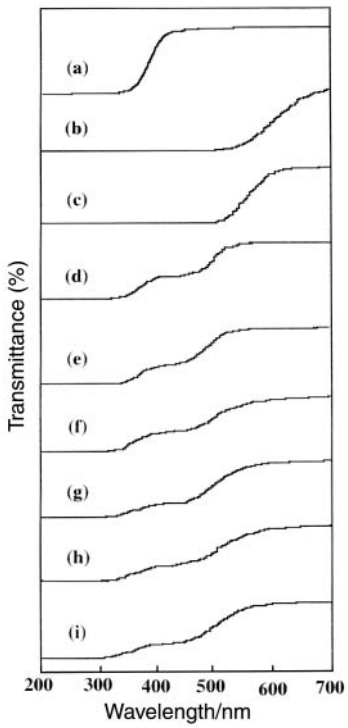

Fig. 4 Reflectance spectra of (a) $HNbWO_6$, (b) CdS, (c) $Cd_{0.8}Zn_{0.2}S$, (d) $HNbWO_6/CdS^*$, (e) $HNbWO_6$/$Cd_{0.8}Zn_{0.2}S^*$, (f) $HNbWO_6$/CdS, (g) $HNbWO_6$/$Cd_{0.8}Zn_{0.2}S$, (h) $HNbWO_6$/(Pt, CdS) and (i) $HNbWO_6$/(Pt, $Cd_{0.8}Zn_{0.2}S$).

Table 1 Gallery height, element content, band gap energy and surface area of the samples

Sample	Gallery height/nm	Content (wt%)			Band gap energy/eV	Surface area/$m^2\ g^{-1}$
		Cd	Zn	Pt		
$HNbWO_6$	0.28	0	0	0	3.06	4.22
CdS		77.7	0	0	1.99	
$Cd_{0.8}Zn_{0.2}S$		70.9	9.0	0	2.11	
$HNbWO_6$/CdS*	0.39	8.4	0	0	2.38, 3.16	6.05
$HNbWO_6$/$Cd_{0.8}Zn_{0.2}S$*	0.38	6.8	1.0	0	2.38, 3.20	8.02
$HNbWO_6$/CdS	0.39	12.2	0	0	2.25, 3.22	9.49
$HNbWO_6$/$Cd_{0.8}Zn_{0.2}S$	0.38	9.0	3.8	0	2.28, 3.28	9.93
$HNbWO_6$/(Pt, CdS)	0.39	12.1	0	2.2	2.19, 3.18	10.78
$HNbWO_6$/(Pt, $Cd_{0.8}Zn_{0.2}S$)	0.38	8.8	3.6	1.4	2.17, 3.22	11.97

and $HNbWO_6$/(Pt, $Cd_{0.8}Zn_{0.2}S$) indicate the different characteristics of CdS and $Cd_{0.8}Zn_{0.2}S$ particles in these nanocomposites, although they have similar interlayer distances.

The interlayer distances, Cd, Zn and Pt contents, band gap energies and specific surface areas of the products are summarized in Table 1. The specific surface areas of $HNbWO_6$/CdS, $HNbWO_6$/$Cd_{0.8}Zn_{0.2}S$, $HNbWO_6$/(Pt, CdS) and $HNbWO_6$/(Pt, $Cd_{0.8}Zn_{0.2}S$) are twice as large as that of $HNbWO_6$ which further indicates the intercalation of CdS and $Cd_{0.8}Zn_{0.2}S$ and the formation of the pillars. Smaller specific surface areas seen in $HNbWO_6$/CdS^* and $HNbWO_6$/$Cd_{0.8}Zn_{0.2}S^*$ compared with $HNbWO_6$/CdS and $HNbWO_6$/$Cd_{0.8}Zn_{0.2}S$ are also due to the ion intercalation of Cd^{2+} and Zn^{2+}, followed by the incorporation of CdS and ZnS, are promoted by the pre-expansion of n-$C_3H_7NH_2$.

3.3 Photocatalytic properties

Fig. 5 shows the amount of hydrogen gas produced from 1250 ml aliquots of 0.1 M Na_2S solution containing 1 g of dispersed unsupported CdS, unsupported $Cd_{0.8}Zn_{0.2}S$, $HNbWO_6$/CdS^*, $HNbWO_6$/$Cd_{0.8}Zn_{0.2}S^*$, $HNbWO_6$/CdS, $HNbWO_6$/$Cd_{0.8}Zn_{0.2}S$, $HNbWO_6$/(Pt, CdS) and $HNbWO_6$/(Pt, $Cd_{0.8}Zn_{0.2}S$) at 60°C for 5 h under irradiation with $\lambda > 290$ nm and >400 nm from a 450 W mercury lamp. As expected from their band gap energies (<3 eV), all samples show photocatalytic activities sufficient for the evolution of hydrogen gas by band gap irradiation in the presence of Na_2S as a sacrificial hole acceptor. The quantum yield is estimated at over 10% using the intercalated compounds as catalysts, the sequence of hydrogen production ability being the same under irradiation with $\lambda > 290$ nm and >400 nm, where the photocatalytic activity

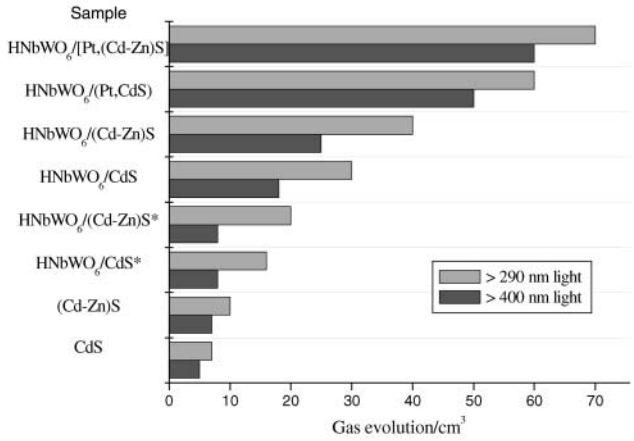

Fig. 5 Amount of hydrogen gas produced from 1250 ml samples of 0.1 M Na_2S solution containing 1 g of dispersed unsupported CdS, unsupported $Cd_{0.8}Zn_{0.2}S$, $HNbWO_6$/CdS^*, $HNbWO_6$/$Cd_{0.8}Zn_{0.2}S^*$, $HNbWO_6$/CdS, $HNbWO_6$/$Cd_{0.8}Zn_{0.2}S$, $HNbWO_6$/(Pt, CdS), $HNbWO_6$/(Pt, $Cd_{0.8}Zn_{0.2}S$) at 60 C for 5 h under irradiation with $\lambda > 290$ nm and >400 nm from a 450 W mercury arc lamp.

increased in the sequence

unsupported CdS < unsupported $Cd_{0.8}Zn_{0.2}S$ < $HNbWO_6$/CdS^* < $HNbWO_6$/$Cd_{0.8}Zn_{0.2}S^*$ < $HNbWO_6$/CdS < $HNbWO_6$/$Cd_{0.8}Zn_{0.2}S$ < $HNbWO_6$/(Pt, CdS) < $HNbWO_6$/(Pt, $Cd_{0.8}Zn_{0.2}S$)

It is notable that the evolution of hydrogen gas in the presence of $HNbWO_6$/CdS and $HNbWO_6$/$Cd_{0.8}Zn_{0.2}S$ is 4–5 times greater than that of unsupported CdS and $Cd_{0.8}Zn_{0.2}S$, and is further enhanced by co-intercalation of Pt with them. The above phenomenon may be explained according to the following reaction mechanism:[16]

$$CdS + 8h\nu \rightarrow 8e^- + 8P^+$$

$$8e^- + 8H_2O \rightarrow 4H_2 + 8OH^-$$

$$8P^+ + S^{2-} + 4H_2O \rightarrow SO_4^{2-} + 8H^+$$

$$8H^+ + 8OH^- \rightarrow 8H_2O$$

The overall reaction is

$$S^{2-} + 4H_2O + 8h\nu \rightarrow SO_4^{2-} + 4H_2$$

The electrons and holes produced by light irradiation easily recombine in unsupported CdS and $Cd_{0.8}Zn_{0.2}S$, but transfer from CdS to the host layer $HNbWO_6$ in $HNbWO_6$/CdS and $HNbWO_6$/$Cd_{0.8}Zn_{0.2}S$ which results in their enhancement of photocatalytic activity, especially when promoted by Pt. Similar results have been reported in Fe_2O_3–Pt–$H_4Nb_6O_{17}$ and Fe_2O_3–Pt–$H_2Ti_4O_9$ systems.[9,10]

It is also found that the hydrogen evolution activities of $HNbWO_6$/$Cd_{0.8}Zn_{0.2}S^*$, $HNbWO_6$/$Cd_{0.8}Zn_{0.2}S$ and $HNbWO_6$/(Pt, $Cd_{0.8}Zn_{0.2}S$) are higher than those of $HNbWO_6$/CdS^*, $HNbWO_6$/CdS and $HNbWO_6$/(Pt, CdS), respectively. The improvement of photoactivity for $Cd_{0.8}Zn_{0.2}S$ systems might be due to the electrons photoinduced transferring from CdS to the ZnS particle while the holes remain in the CdS particle, resulting in the depression of recombination of electrons and holes photoinduced and the enhancement of the photocatalytic activity of the nanocomposite, just as was observed in colloidal CdS–TiO_2 systems[2–4] and the $H_2Ti_4O_9$/CdS–ZnS system.[11,12]

The effect of semiconductor intercalation on the photoactivity of nanocomposites was investigated by loading CdS and $Cd_{0.8}Zn_{0.2}S$ by two different methods, *i.e.* Cd^{2+} and Cd^{2+}–Zn^{2+} were incorporated into the interlayer of $HNbWO_6$ by the reactions of Cd^{2+}–Zn^{2+} with $HNbWO_6$ for $HNbWO_6$/CdS^* and $HNbWO_6$/$Cd_{0.8}Zn_{0.2}S^*$, and by the reactions of $HNbWO_6$/n-$C_3H_7NH_2$ with Cd^{2+} and Cd^{2+}–Zn^{2+} for $HNbWO_6$/CdS and $HNbWO_6$/$Cd_{0.8}Zn_{0.2}S$. Hydrogen gas production from $HNbWO_6$/CdS and $HNbWO_6$/$Cd_{0.8}Zn_{0.2}S$ was larger than that from $HNbWO_6$/$CdS^*$and $HNbWO_6$/$Cd_{0.8}Zn_{0.2}S^*$, respectively. It is suggested that more effective and larger amounts of CdS and $Cd_{0.8}Zn_{0.2}S$ are incorporated into the interlayer of $HNbWO_6$ by pre-expansion of $C_3H_7NH_2$ than are intercalated by general methods.

4 Conclusions

From the results of the tests described the following conclusions may be drawn. (1) $Cd_{0.8}Zn_{0.2}S$ together with Pt could be incorporated into the interlayer of $HNbWO_6$ by successive reaction of $HNbWO_6$ with $[Pt(NH_3)_4]Cl_2$ in aqueous solution, with n-$C_3H_7NH_2$/n-heptane in organic solution and with the $Cd(MeCO_2)_2$–$Zn(MeCO_2)_2$ mixture in aqueous solution, followed by the reaction between Cd^{2+}–Zn^{2+} and H_2S in the interlayer of $HNbWO_6$. (2) The intercalated layer distances of $HNbWO_6$/CdS, $HNbWO_6$/$Cd_{0.8}Zn_{0.2}S$, $HNbWO_6$/CdS*, $HNbWO_6$/$Cd_{0.8}Zn_{0.2}S$*, $HNbWO_6$/(Pt, CdS) and $HNbWO_6$/(Pt, $Cd_{0.8}Zn_{0.2}S$) nanocomposites are less than 0.5 nm. (3) $HNbWO_6$/(Pt, $Cd_{0.8}Zn_{0.2}S$) nanocomposite series show hydrogen production activities under irradiation with $\lambda > 290$ nm and > 400 nm in the presence of Na_2S as a sacrificial hole acceptor. The photocatalytic activities of $HNbWO_6$/CdS and $HNbWO_6$/$Cd_{0.8}Zn_{0.2}S$ nanocomposites are superior to those of unsupported CdS and $Cd_{0.8}Zn_{0.2}S$ and are enhanced by the co-incorporation of Pt.

Acknowledgements

This work was jointly supported by the National Natural Science Foundation of China (No. 50082003), Provincial Natural Science Foundation of Fujian, China (No. F992001) and a Grant-in-Aid for Scientific Research from the Ministry of Education, Science and Culture of Japan.

References

1 U. Bjorksten, J. Moser and M. Gratzel, *Chem. Mater.*, 1994, **6**, 858.
2 K. R. Gopidas, M. Bohorquez and P. V. Kamat, *J. Phys. Chem.*, 1990, **94**, 6435.
3 N. Serpone, E. Borgarello and M. Gratzel, *J. Chem. Soc., Chem. Commun.*, 1983, 342.
4 L. Spanhel and H. Henglein, *J. Am. Chem. Soc.*, 1987, **109**, 6632.
5 O. Enea and A. J. Bard, *J. Phys. Chem.*, 1986, **90**, 301.
6 H. Miyoshi and H. Yoneyama, *J. Chem. Soc., Faraday Trans.*, 1989, **85**, 1873.
7 H. Yoneyama, S. Haga and S. Yamanaka, *J. Phys. Chem.*, 1989, **93**, 4833.
8 H. Miyoshi, H. Mori and H. Yoneyama, *Langmuir*, 1991, **7**, 503.
9 T. Sato, Y. Yamamoto and S. Uchida, *J. Chem. Soc., Faraday Trans.*, 1996, **92**, 5089.
10 S. Uchida, Y. Yamamoto and T. Sato, *J. Chem. Soc., Faraday Trans.*, 1997, **93**, 3229.
11 J.-H. Wu, S. Uchida, Y. Fujishiro, S. Yin and T. Sato, *J. Photochem. Photobiol., A*, 1999, **128**, 129.
12 J.-H. Wu, S. Uchida, Y. Fujishiro, S. Yin and T. Sato, *Int. J. Inorg. Mater.*, 1999, **1**, 253.
13 V. Bhat and J. Gopalakrishnan, *Solid State Ionics*, 1988, **26**, 25.
14 R. P. Shannon and C. T. Prewitt, *Acta Crystallogr., Sect. B*, 1961, **25**, 125.
15 A. Hagfeldt and M. Gratzel, *Chem. Rev.*, 1995, **95**, 49.
16 T. Sato, K. Masaki and K. Sato, *J. Chem. Technol. Biotechnol.*, 1996, **67**, 339.